17th Australasian Fluid Mechanics Conference
Auckland, New Zealand
5-9 December 2010

Dense Gravity Currents in a Rotating, Adverse, Converging Channel

A.J.S Cuthbertson[1], P.A. Davies[1], J. Laanearu[2] and A.K. Wåhlin[3]

[1]Department of Civil Engineering
University of Dundee, Dundee DD1 4HN, UK

[2]Institute of Mechanics
Tallinn University of Technology, 19086, Tallinn, Estonia

[3]Department of Earth Sciences
University of Gothenburg, 405 30 Gothenburg, Sweden

Abstract

Results are presented from a series of laboratory experiments on dense bottom gravity currents in an inclined, submerged, rotating and convergent vee-shaped channel. Density and velocity profile measurements across and along the channel are compared with theoretical model predictions based upon rotating (inviscid) hydraulics and Ekman dynamics, respectively. Good qualitative agreement is demonstrated, with quantitative discrepancies attributed to turbulent entrainment and mixing processes omitted from the theoretical models.

Introduction

Gravity currents in rotating systems have wide environmental and geophysical relevance, particularly for dense oceanic and estuarine/fjord outflows affected by the Earth's rotation where bottom bathymetry exerts crucial controls on the velocity and density fields within the flow (e.g Borenäs & Lundberg [1]). Knowledge of these effects is inadequate, especially with regard to (i) the maintenance of geostrophic balance within outflows confined by complex bottom topography, (ii) the prediction of slope, distortion and elevation of the interface between the intrusive dense outflow layer and the overlying, relatively-quiescent receiving waters and (iii) the limiting and restricting effects of hydraulic control and transport capacity (Wåhlin [6]) on the outflow dynamics.

Physical System

The laboratory configuration shown in Figure 1 is an idealised representation of an oceanic outflow along an up-sloping and converging deep submarine channel approaching a submerged sill crest (Girton *et al* [5]; Borenäs and Lundberg [1]). The model topography consists of a symmetric, vee-shaped channel with variable side slope angles $\alpha(y)$ and an along-channel bed slope S_0, inclined upwards towards the channel exit. The Cartesian coordinate system (x, y, z) is orientated with x and y axes in the cross- and along-channel directions, respectively, and the z axis taken as anti-parallel to the gravitational acceleration vector $\mathbf{g}$ = (0, 0, -g). The initial, undisturbed configuration is one in which the channel topography is submerged within a homogeneous ambient fluid of density ρ_0 and depth H in a state of solid body rotation with angular velocity $\boldsymbol{\Omega}$ = (0, 0, Ω). At time t = 0, a dense water source flow, having typical horizontal and vertical inflow dimensions l_0 and h_0, density $\rho_1 = [\rho_0 + (\Delta\rho)_0]$, dynamic viscosity μ and initial volume flux Q_0 is introduced upstream of the constant width section of the channel. The model dynamical parameters have been chosen to match the ranges observed in oceanic dense outflows

Laboratory experiments

The experiments utilised a 5 m diameter by 0.5 m-deep circular rotating tank of fresh water in which the model topography was submerged and set with bed slope S_0 (= 1.7°, 3.6°). With the water spun-up to solid-body rotation at a prescribed angular velocity Ω, brine of prescribed density ρ_1 was introduced at the upstream end of the channel with volume flux Q_0 that was increased incrementally at prescribed normalised elapsed times $2\Omega t$ during each experimental run.

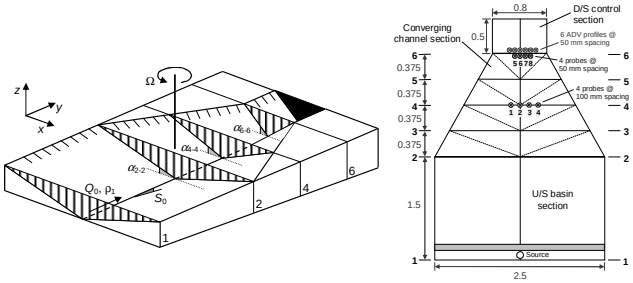

Figure 1. Sketch and plan view of the rotating, converging channel.

Vertical density profiles were taken at pre-set sampling frequencies at fixed locations within the channel using micro-conductivity probes mounted on motorised rack systems controlled by computer (Cuthbertson *et al* [3]). Two profiling rigs were sited at sections 4 and 6, each with four probes (denoted P1 – P4 and P5 – P8) at fixed cross-channel measurement locations (figure 1). Velocity measurements for each outflow condition were obtained using an acoustic Doppler velocimeter (ADV) mounted on a motorised traversing system.

Results

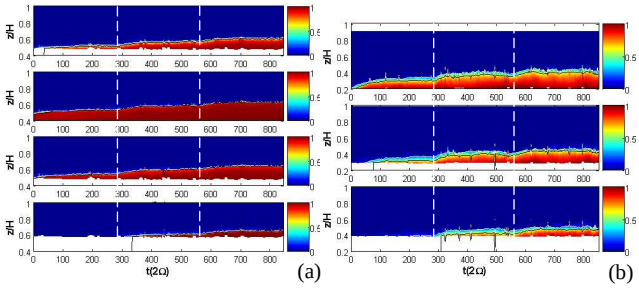

Figure 2. Time sequences of density profiles at section 6 for (a) S_0 = 3.6°; Bu = 0.23, 0.20, 0.19 (probes P5-P8) and (b) S_0 = 1.7°; Bu = 0.27, 0.30, 0.39 (probes P6-P8). Here, Burger number $Bu = g(\Delta\rho)_0 h_0/\rho_0 l_0^2(2\Omega)^2$.

Figure 2 shows typical time series plotted non-dimensionally as density excess $\rho' = (\rho - \rho_0)/(\Delta\rho)_0$ within the normalised time-($2\Omega t$) space (z/H) domain, at the downstream locations [P5 – P8]. The dashed white lines in Figure 2 indicate the times at which Q_0 (and Bu, through the dependence of h_0 and l_0 upon Q_0) was increased incrementally during the experimental runs. For all S_0 = 3.6° runs, the interface between the dense water outflow ($\rho' \rightarrow 1$) and overlying ambient fluid ($\rho' = 0$) remains sharply defined throughout the experiment. The temporal development of the dense outflow layer also indicates well-defined increases in interface elevation corresponding to the incremental increases in Q_0. After each adjustment, fully developed outflow conditions are typically established along the channel. For S_0 = 1.7° and Bu varying between 0.27 and 0.39, the plots show a more diffuse interface forming between the outflowing dense bottom water and overlying ambient fluid layer, due to significant shear-induced interfacial mixing. Cross-channel interface slopes α_i, derived from measured isopycnal elevations (typified by Figure 3) are shown to agree well (see Figure 4) with assumptions of geostrophy along the channel. This implies a slope $\alpha_g = (2\Omega)V/g'$, where V is the depth-averaged outflow velocity (measured by ADV) and $g' = g(\Delta\rho)/\rho_0$ is the local, modified gravitational acceleration based upon local, measured density profiles.

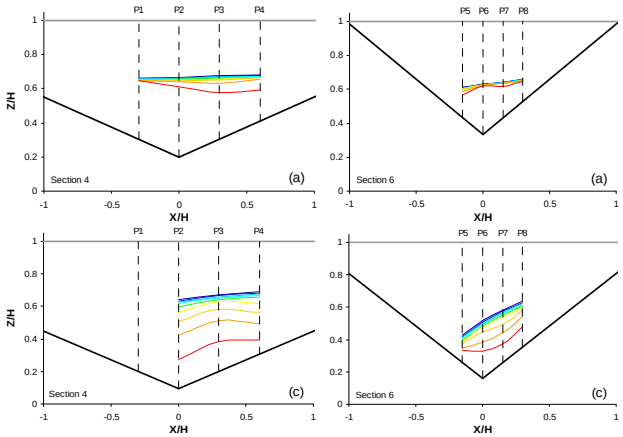

Figure 3. Cross-channel isopycnals ρ′ = 0.1 (blue) – 0.9 (red) at sections 4 and 6 for runs with S_0: Bu values (a) 3.6°: 0.190, (c) 1.7°: 0.03

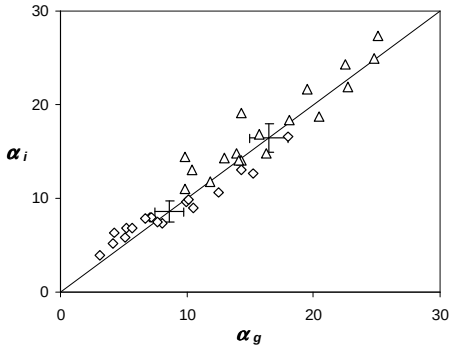

Figure 4. Composite data comparisons of measured (α_i) and computed geostrophic (α_g) slopes (◊ and Δ are S_0 = 3.6° and 1.7°, respectively)

Cross- and along-channel velocities were measured directly within the dense layer: Figure 5 shows typical ADV profiles of the along- $v(x,z)$ and cross- $u(x,z)$ channel velocities for 3 separate runs. These plots show clearly that the magnitude of the along-channel velocity within the outflowing dense water layer is relatively high compared to the passive conditions typically observed within the overlying ambient water layer. The plots also indicate that the maximum along-channel outflow velocities v_{max} occur at or close to the channel centreline ($x/H \approx 0$) in all cases, while diminishing in magnitude at more outlying measurement locations where the outflow layer thickness also diminishes. Comparison of Figures 5(a) and (b) highlights the influence of longitudinal bed slope S_0 on the along-channel velocities for otherwise-identical Bu conditions. In particular, it is apparent that the magnitude of v values in the outflowing layer (at equivalent lateral x/H positions) is notably higher at the lower bed slope S_0 = 1.7°; a property that is reflected in the increased levels of shear-induced mixing specifically observed in these runs.

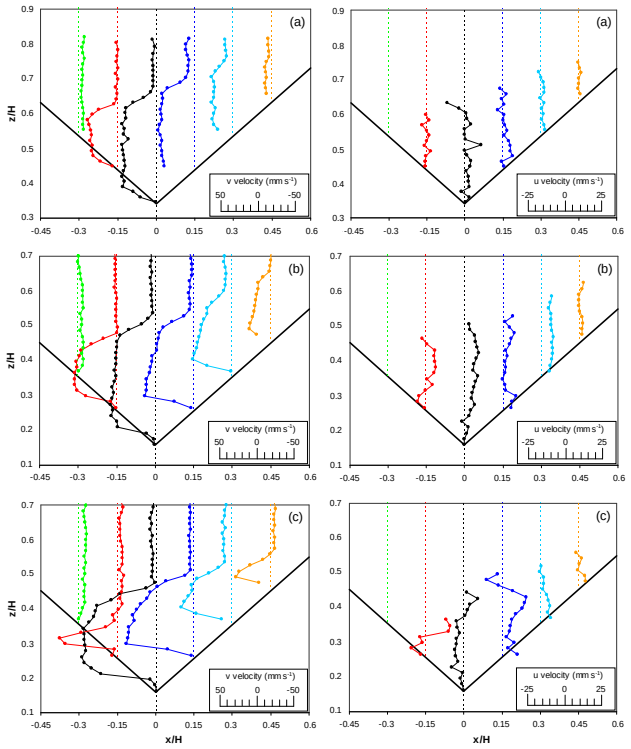

Figure 5. Typical plots of along- $v(x,z)$ and cross- $u(x,z)$ channel velocity profiles at section 6 for S_0: Bu (a) 3.6°: 0.02, (b) 1.7°: 0.03, (c) 1.7°: 0.12

Similar comparisons between the Figures 5(b) and 5(c) highlight the effects on the along-channel outflow velocities of increasing the relative influence of stratification over rotation. Specifically, while the v values in the outflow layer increase at all x/H locations, the corresponding layer thickness diminishes significantly. Cross-channel $u(x,z)$ profiles within the outflowing dense water layers indicate that fluid motion is to the right (looking downstream) with $u(z) > 0$. This secondary flow is especially evident in the S_0 = 1.7° runs (Figures 5(b) and (c)), although it remains relatively small in magnitude compared to the v-component outflow velocities. In these aspects, the observed characteristics of cross-channel motion within the outflow layer are in qualitative agreement with the secondary return flow mechanism proposed by Davies *et al* [4] for a gravity current descending down an inclined, rotating and diverging v-shaped channel.

Theoretical Considerations

Inviscid hydraulics

The model developed by Borenäs & Lundberg (1986, 1988) to describe the hydraulics of rotating, inviscid, dense outflows may be applied to the above flow. By conservation of potential vorticity,

$$\frac{d}{dt}\left(\frac{\omega_z + f}{h}\right) = 0 \qquad (1)$$

where ω_z is the vertical component of relative vorticity of the disturbance flow, h is the (variable) dense fluid depth and f (= 2Ω) is the Coriolis parameter. In a channel where along-channel variations are much smaller than cross-channel variations [$\partial/\partial y << \partial/\partial x$], the cross-channel component of the momentum equation reduces to the geostrophic balance for the along-channel velocity $v(x)$, such that

$$f\, v(x) = g' \frac{\partial h}{\partial x} \tag{2}$$

where g' is the modified gravitational acceleration defined earlier. Furthermore, for an inviscid flow, the potential vorticity is conserved along a streamline and equation (2) can be simplified to

$$\frac{f + \partial v/\partial x}{h} = \frac{f}{h_\infty} \tag{3}$$

where h_∞ is the potential depth [i.e. the depth at which relative vorticity ($\partial v/\partial x$) vanishes], which, for the purposes of comparison with the laboratory model results, is fixed at $h_\infty = H/2$ for all computations. A solution for the interface height $h(x)$ can be derived from equations (3) and (4) by exploiting the conservation of specific energy along the streamlines, yielding for a triangular cross-section channel:

$$h(x) = \frac{(h_\infty - 2\alpha a)}{\sinh((a+b)/\lambda)}\left[\sinh\left(\frac{x-b}{\lambda}\right) - \sinh\left(\frac{a+x}{\lambda}\right)\right] - 2\alpha a \frac{\sinh((a+x)/\lambda)}{\sinh((a+b)/\lambda)} + (h_\infty - z_s + \alpha x) \tag{4}$$

where x = ($-a$, b) represents the lateral coordinates of the intersection with the channel bed of the interface between the dense gravity current and the overlying, quiescent receiving fluid (see Figure 3), $\lambda = (g'h_\infty)^{1/2}/f$ is the Rossby radius of deformation based on the potential depth h_∞ and z_s is the sill elevation. The geostrophic velocity $v(x)$ can be found directly from equations (3) and (5), with the geostrophic transport maximum determined by the critical flow variables x = (a_{crit}, b_{crit}) corresponding to the appropriate Froude number condition $Fr^* = 1$ for the rotating triangular channel topography (see Borenäs & Lundberg, 1986), such that:

$$Fr^{*2} = \bar{v}^2 \Big/ \left[\left(\hat{v} + \hat{D}_\infty \coth\left(\frac{a+b}{2\lambda}\right)\right)\left(\hat{v} + \hat{D}_\infty \tanh\left(\frac{a+b}{2\lambda}\right)\right)\right]$$
$$\bar{v} = \frac{g'\alpha}{f}\left(1 - \frac{a}{\lambda}\coth\left(\frac{a+b}{2\lambda}\right)\right)$$
$$\hat{v} = \frac{g'\alpha}{f}\left(\frac{a}{\lambda} - \frac{D_\infty}{k\lambda}\tanh\left(\frac{a+b}{2\lambda}\right)\right) \tag{5}$$

where the tilde symbols on h and D denote dimensionless potential and deep water depths respectively, in terms of λ. The solutions obtained from equations (3) – (6) thus correspond to critical flow conditions, within which the maximum geostrophic flow is fitted, in turn, to each of the different experimental flow rates specified by the laboratory model conditions.

Ekman dynamics

Previous treatments of frictional controls of dense outflows in rotating channel geometries have utilised an Ekman layer model (Davies *et al*. [4]) in which the dynamic balance is between the effects of along- and cross-pressure gradients, Coriolis acceleration and bottom friction (Davies *et al*. [4]). As demonstrated by Wåhlin & Walin [8], bottom friction can be represented either as a bulk drag force acting on the main flow or by resolving the Ekman spiral, so long as the drag coefficient is chosen such that the net frictional force is equal in the different representations. The Ekman layer solution may be written conveniently as follows:

$$u = u_g\left[1 - e^{-\frac{z}{2\delta}}\cos\left(\frac{z}{2\delta}\right)\right] - v_g e^{-\frac{z}{2\delta}}\sin\left(\frac{z}{2\delta}\right)$$
$$v = v_g\left[1 - e^{-\frac{z}{2\delta}}\cos\left(\frac{z}{2\delta}\right)\right] + u_g e^{-\frac{z}{2\delta}}\sin\left(\frac{z}{2\delta}\right) \tag{6}$$

where $\delta = (\upsilon/2f)^{1/2}$ is the thickness of the Ekman layer, υ is the kinematic viscosity and (u_g, v_g) are the geostrophic velocities in the (x, y) directions (Davies *et al*. [4]). For the case of a moving lower dense layer and an overlying quiescent, upper ambient layer, with the assumption of $\partial v/\partial x << f$ and $\partial/\partial y << \partial/\partial x$, a frictionally-controlled system can be derived and solved with respect to the dense layer thickness $h(x,y)$. Solutions for different channel topographies have been obtained (Wåhlin [6]; Wåhlin [7]; Davies *et al*. [4]; Borenäs *et al*. [2]). For example, for a dense gravity current flowing down an inclined, vee-shaped channel (Davies *et al*. [4]):

$$h(x) = \frac{\delta\alpha}{\phi}\left[(A+2)e^{x\frac{\phi}{\delta}} - 1\right] \qquad x < 0$$
$$h(x) = \frac{\delta\alpha}{\phi}\left(Ae^{x\frac{\phi}{\delta}} + 1\right) \qquad x \geq 0 \tag{7}$$

where h is the thickness of the outflowing dense layer, ϕ is the along-channel interface slope and A is an integration constant determined from boundary conditions. Horizontal integration of the quantity vh across the channel gives the along-channel transport flux Q according to

$$Q = \int_a^b vh\,dx = \int_a^0 vh\,dx + \int_0^b vh\,dx = \frac{g'}{f}\frac{\delta^2\alpha^2}{\phi^2}Q_F(A)$$
$$Q_F(A) = \left[-2A - 2 + \ln\left(-1 - \frac{2}{A}\right)\right] \tag{8}$$

where integral limits $x = a$ and $x = b$ are the interface/side-slope intersections (as defined earlier). In this case, the along-channel slope of the interface has previously either been assumed equal to the slope of the channel (or canyon) axis. However, for the up-sloping, vee-channel configuration here, both A and ϕ have to be determined using two prescribed conditions, namely (i) the right-hand intersection between the outflow layer and channel bed boundary (looking downstream) is horizontal, and (ii) the along-channel transport is equal to the source transport flux Q_0. The first condition can be written as follows

$$h(b) + z_b(b) = h_0 \tag{9}$$

where $h(b)$ and $z_b(b)$ are respectively the outflow layer thickness and bed elevation at $x = b$, is the upstream outflow layer thickness. Using equation (9) in (7) gives the condition for A, i.e.

$$A = -e^{\frac{\phi}{\delta}z_b(x=0)} \tag{10}$$

Substitution of equation (10) into (8) provides two roots of ϕ for each Q_0 value, the smaller of the two roots being chosen on physical grounds to permit both the along- and cross-channel interface slopes to increase as the downstream end section of the channel is approached. Solutions for $h(x)$ (and hence α_i) can then

be obtained from equation (7) and compared with corresponding laboratory measurements.

C**omparisons**

Figure 6 shows comparisons between the measured and predicted cross-channel variation in interface elevation at sections 4 and 6. Corresponding comparisons of outflow layer thickness h_i and cross-channel interface slope α_i are presented in figures 7(a) and (b), respectively. The predictions of interface elevation by the Ekman dynamics friction model (EDFM) at section 4 (see Figure 1) are shown to be consistently close to (but lower than) the measured interface elevations (with correspondingly lower h_i values, see Figure 7(a)). By contrast, corresponding EDFM predictions at the channel exit (Section 6), are significantly higher than observed in the experiments. This discrepancy relates to the required specification of the upstream elevation h_0 of the interface and a fixed value for the along-channel slope ϕ [equations (9) and (7), respectively] as input parameters. The inviscid, rotating hydraulic model (IRHM) predicts significantly lower values of interface elevation (figure 6) and outflow layer thickness h_i (Figure 7(a)) than experimental measurements at section 6. This is attributed to the frictionless bottom condition adopted in the IRHM approach, which reduces the flow area (and hence h_i) required for the critical and maximal discharge conditions to develop at the downstream control section within the channel.

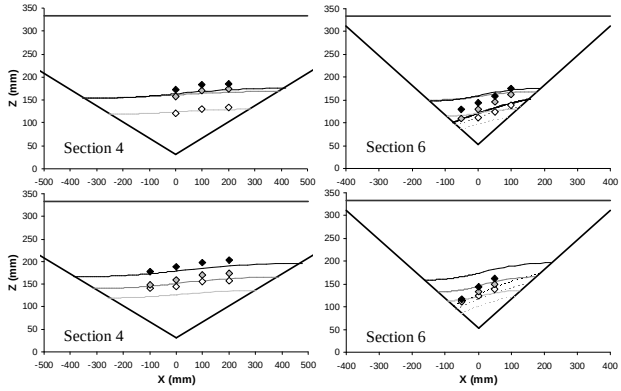

Figure 6. Comparisons of interfacial profiles (density) at sections 4 and 6, showing data points (symbols) and predicted profiles from Ekman (solid) and inviscid hydraulics (dashed) theories, for S_0: $(g')_0$: f values of 1.7°: 0.189 m.s^{-2}: 0.417 s^{-1} (top) and 1.7°: 0.122 m.s^{-2}: 0.417 s^{-1} (bottom).

Comparisons between the measured and predicted values of cross-channel interface slope α_i (Figure 7(b)) show both EDFM and IRHM approaches underestimating α_i at both sections (IRHM at section 6 only). These discrepancies are ascribed to the significant shear-induced mixing observed in the S_0 = 1.7° runs, a process that is not incorporated in either of the models.

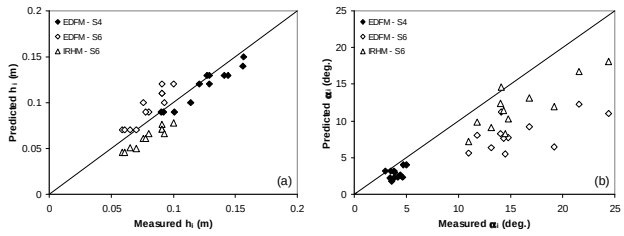

Figure 7. Comparison of experimental measurements and theoretical predictions of (a) maximum outflow layer thickness h_i and (ii) cross-channel interface slope α_i at sections 4 and 6

Predictions of α_i could thus be improved by calculating an outflow-layer-averaged value of g' (e.g. Girton *et al*. [5]) to take account of local density stratification characteristics due to mixing along the channel. Further, some of the divergence between the model predictions and experimental data arises from the arbitrary selection of the reference isopycnal to represent the measured interface elevation.

Conclusions

Comparisons between the laboratory results and the application of rotating, inviscid hydraulics theory and Ekman dynamics demonstrate that the qualitative aspects of the dense outflows are captured well by the complementary predictions of theory. Inviscid, rotating hydraulics theory for critical flow conditions at the exit section underestimates the deep-layer depth h_i and the cross-channel interface slope α_i but this discrepancy may be attributed primarily to the absence in the model of frictional effects at the channel boundaries and the layer interface. The incorporation of frictional effects through Ekman dynamics results in improvement in agreement between theoretical prediction of the parametric dependence of the outflow characteristics, though the absence of any interfacial mixing processes in either of the theoretical models results in quantitative discrepancies between theory and experiment. The laboratory data demonstrate that shear-induced entrainment and turbulent mixing across the interface is a common feature for the parameter ranges of interest here.

Acknowledgments

This work has been supported by the European Community's Sixth Framework Programme through the grant to the budget of the Integrated Infrastructure Initiative HYDRALAB III within the Transnational Access Activities, Contract no. 022441. The authors would like to thank Dr. Thomas McClimans and his colleagues at the Norwegian University of Science & Technology (SINTEF) for their hospitality and technical assistance.

References

[1] Borenäs, K. & Lundberg, P., The Faroe-Bank Channel deep-water overflow, *Deep-Sea Res.,* **51**, 2004, 335-350..

[2] Borenäs, K., Hietala, R., Laanearu, J. & Lundberg, P., Some estimates of the Baltic deep-water transport through the Stolpe trench, *Tellus A*, 59, 2007, 238-248.

[3] Cuthbertson, A. J. S., Davies, P. A., Coates, M. J. & Guo, Y., A modelling study of transient, buoyancy-driven exchange flow over a descending barrier, *Env. Fluid Mech.*, **4**, 2004, 127-155.

[4] Davies, P. A., Wåhlin, A. K. & Guo, Y., A combined laboratory and analytical study of flow through the Faroe Bank Channel, *J. Phys. Oceanogr.*, **36**, 2006, 1348-1364.

[5] Girton, J. B., Pratt, L. J., Sutherland, D. A. and Price, J. F., Is the Faroe Bank Channel overflow hydraulically controlled? *J. Phys. Oceanogr.*, **36**, 2006, 2340-2349.

[6] Wåhlin, A. K., Topographic steering of dense bottom currents with application to submarine canyons, *Deep-Sea Res.*, **49**, 2002, 305 – 320.

[7] Wåhlin, A. K., Downward channelling of dense water in topographic corrugations, *Deep Sea Res.*, **51**, 2004, 577-599.

[8] Wåhlin, A. K. & Walin, G., Downward migration of dense bottom currents. *Env. Fluid Mech.*, **1**, 2001, 257 – 279.